Surface plasmon polaritons launched using a terahertz free-electron laser: propagation along a gold–ZnS–air interface and decoupling to free waves at the surface edge

Vasily V. Gerasimov,[1,2] Boris A. Knyazev,[1,2,*] Igor A. Kotelnikov,[1,2] Alexey K. Nikitin,[2,3] Valery S. Cherkassky,[2] Gennady N. Kulipanov,[1] and Guerman N. Zhizhin[3]

[1]*Budker Institute of Nuclear Physics SB RAS, 11 Lavrentyev Avenue, Novosibirsk 630090, Russia*
[2]*Novosibirsk State University, 2 Pirogova Street, Novosibirsk 630090, Russia*
[3]*Scientific and Technological Center for Unique Instrumentation of RAS, 15 Butlerova Street, Moscow 117342, Russia*
**Corresponding author: Ba_knyazev@phys.nsu.ru*

Received March 1, 2013; accepted May 31, 2013;
posted June 17, 2013 (Doc. ID 186086); published July 18, 2013

In this paper, we experimentally study the propagation of surface plasmon polaritons (SPPs) along gold–ZnS–air interfaces and their diffraction at the surface edge. The SPPs were launched by the waveguide method using monochromatic radiation of the Novosibirsk Free-Electron Laser, operated at the wavelength 140 μm. SPP characteristics were studied via examination of the electromagnetic field of diffracted waves employing two terahertz sensors: a movable Golay cell and an optical system, consisting of a TPX lens and a 320 × 240 microbolometer focal plane array (MBFPA) recording images with a rate of 17 frames/s. The experimentally recorded intensity distribution of the diffracted wave in the direction normal to the surface differed from the evanescence wave distribution in the SPP, but their characteristic widths were practically the same and coincided with the theoretical calculations made within the Drude model [Phys. Rev. A **87**, 023828 (2013)]. Diffracted wave characteristics drastically changed when ZnS-layer thickness increased from 0 to 0.75 μm. The angular distributions grew from 0.16 to 3.6 deg, but the characteristic beam width decreased from 8 to 0.35 mm, which is promising for a number of applications. The propagation length of SPPs therewith decreased from 31 to 11 mm, which is 3 orders of magnitude less than the Drude theory predicts. Prospects for further studies are discussed.

OCIS codes: (240.6680) Surface plasmons; (300.6495) Spectroscopy, terahertz; (240.0310) Thin films; (110.2970) Image detection systems.
http://dx.doi.org/10.1364/JOSAB.30.002182

1. INTRODUCTION

Surface plasmon polaritons (SPPs) are partially longitudinal *p*-polarized evanescent electromagnetic waves that propagate along a metal–dielectric interface as a result of collective electron oscillations coupled to an external electromagnetic field (EMF) [1–5]. These waves, also known as surface electromagnetic waves, were first analytically investigated by Sommerfeld and Zenneck [6,7], and are often called "Zenneck waves" (see, e.g., [8–10]), but the authors of a recent paper [11] call the existence of surface electromagnetic waves under the conditions described by Zenneck (Earth–air interface) into question. Fano [12] may be the first to describe surface electromagnetic waves on a plane boundary between a dielectric and a medium with a negative dielectric constant, and the term "Fano waves" can be also found in the literature (see, e.g., [13,14]). The amplitude of these waves is maximal at the surface and decays exponentially with different decay constants in the directions parallel and perpendicular to the boundary. Most of the field energy is concentrated in the dielectric in the immediate vicinity of the metal and increases with the wavelength. Propagation of surface waves along plane metal surfaces with absorbing layers was studied both theoretically and numerically in [15]. The calculations had shown that the length of SPP propagation is rather sensitive to absorbing layers covering the metal surface. This feature of SPPs provides a possibility for their use in the spectroscopy of conducting surfaces and thin films.

The propagation length L for plasmons in the visible range is a few tens of micrometers [3,16], which is close to the values calculated using the Drude theory. In accordance with the theory, the propagation length must grow with the wavelength as λ^2, reaching a magnitude of several meters in the terahertz range (see Fig. 5 in [17]). No one experiment, however, has confirmed this prediction, and propagation lengths that were measured experimentally in the far-infrared are much shorter—by many orders of magnitude—than the expected ones. No satisfying explanation for this fact has been given so far. One of the reasons may be that, in contrast to shortwave ranges, in the terahertz range the phase velocity of SPPs differs from the speed of light in the dielectric by only hundredths of a percent, which may weaken coupling of SPPs to the surface and increase the radiation losses [10]. Another explanation refers to additional electron scattering mechanisms in thin films [18].

The range of possible methods to study terahertz plasmons depends strongly on specific features of sources applied. Initially, terahertz SPPs were studied using submillimeter

gas lasers [19,20]. In the past decades, SPPs in the terahertz range were investigated mostly by using broadband pulsed sources, by the time-domain spectroscopy technique [10,21,22]. In this paper we study SPPs by using high-power monochromatic radiation of the recently commissioned terahertz Novosibirsk Free-Electron Laser (NovoFEL) [23,24].

Since SPP is a nonradiative wave localized near the surface of a conductor, its characteristics are usually studied either by using a material probe [25,26] or via decoupling of a portion of radiation into a bulk wave (BW) using an "inverse transformation element" [27,28]: an attenuated total reflection prism, a grating, a slit, etc. All of these techniques obviously disturb the SPP field, and the information obtained may be incorrect or require careful processing. We used an alternative method for studying SPPs: examination of BWs that arise when a SPP propagating on a thin-film-coated gold sample is diffracted at the sample edge. This method requires sensing of diffracted radiation over a large area and can hardly be realized, for example, with the time-domain spectroscopy technique. This method, however, is easy to implement using a monochromatic terahertz source and rather sensitive sensors and imaging devices.

To process the data obtained with this method, a reliable theory connecting SPP characteristics with the diffractive wave properties is necessary. Most previous simulations of SPP diffraction [29–32] were carried out for different geometries, different interfaces, and different spectral ranges and cannot be directly applied in our case. In [22] a rough estimation of the diffracted field was made using a Huygens scalar model. In [33] the diffraction of a SPP on a conductive wedge was analyzed for infrared radiation using the Sommerfeld–Malyuzhinets approach (see details below). Since no final expression describing the diffracted waves was achieved in the cited paper, the task was reconsidered in detail in the companion paper [34]; those results were used for data processing in our experiments.

In this paper we present the results of an experimental study of SPPs launched using monochromatic terahertz radiation generated by NovoFEL, traveling along a metal–dielectric interface, and decoupling at the sample tail edge. In Section 2 we describe the experimental setup, the method for coupling of laser radiation to SPP at a sample–air interface, characteristics of the samples, and terahertz radiation sensors. Section 3 presents experimentally observed distributions of EMF intensity beyond the rear edge of samples with different layers. The above-mentioned theory for diffraction of SPPs is briefly outlined and compared with the experiment in Sections 4 and 5. Comparison of theoretical predictions with experimental data shows good agreement. This fact permits the study of SPP characteristics via sensing of the diffracted wave. In Section 5, using this method, we present results of the measurements of the SPP propagation length for gold–air and gold–ZnS–air structures. The results of the work are summarized in Section 6.

2. EXPERIMENTAL SETUP

The diagram in Fig. 1 shows a schematic of the experimental setup. The NovoFEL serves as a source of terahertz radiation. It emits a continuous stream of 100 ps pulses with a repetition rate of 5.6 MHz. The radiation wavelength can be precisely tuned within the spectral range of 50–240 μm. Our experiments were carried out at the wavelength $\lambda = 140$ μm with a relative linewidth of 1% or less. The laser radiation was transmitted to the user station through a 15 m optical beamline filled with dry nitrogen. The average power of radiation, arriving at the user station as a Gaussian beam with a waist of 10 mm, was about 10 W in these experiments. The input radiation was plane polarized at 18 deg clockwise from the vertical.

If necessary (see Section 3), a chopper can modulate the laser beam at a frequency of 15 Hz. The beam intensity can be attenuated with a wire polarizer. To monitor variations of laser beam intensity we used polypropylene film beam splitter, which reflected some of the input radiation to a pyroelectric detector. Since only a TM wave (the electric vector lies in the figure plane) can be converted into SPPs, a photolithographic polarizer was used as a TM- or TE-pass (in test experiments) polarizer. After passing 10 mm iris diaphragm, the beam was focused by plane mirror M_1 and cylindrical mirror M_2 ($f = 70$ mm) into the input mouth of the parallel-plate waveguide, similar to the one used in [10] and formed by the conductive surface of a sample under study and a gold-covered glass prism. Though the input laser beam power was high, no damage of the input mouth was observed in any our experiments. Since only a small portion of the input radiation transformed into SPP, we assumed that thermal effects were negligible.

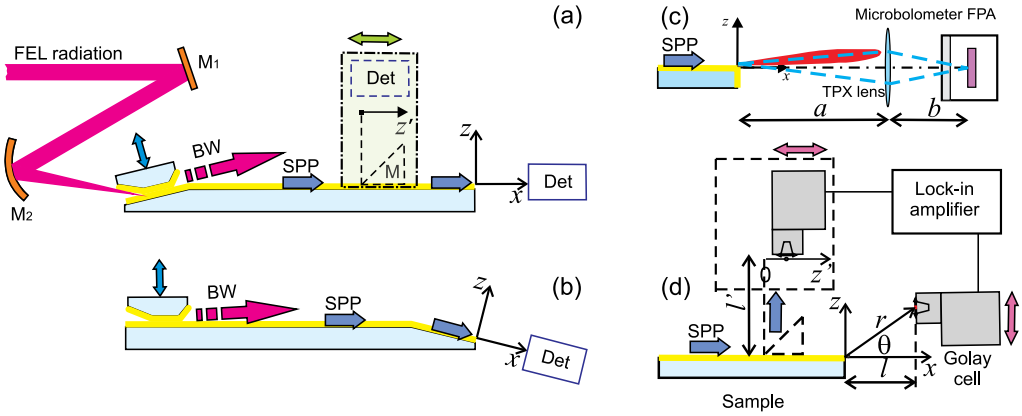

Fig. 1. Experimental configurations: (a) basic configuration and (b) reverse-geometry configuration. Detection systems: (c) imaging system with a TPX lens and a MBFPA and (d) Golay cell with a 0.2 mm wide input slit coupled to a SR-830 lock-in amplifier. The z' axis is the "image" of the z axis in the mirror. The system in the dashed square was used for study of SPP propagation length (see Section 6).

The samples were glass substrates 25 cm long, 4 cm wide, and 1 cm thick with a flat highly polished upper face with deposited a 1 μm thick layer of gold and optionally covered on top with a 0.1–3 μm thick layer of ZnS. For separation of SPP and the (see Fig. 1, a 4 cm portion of each substrate was ground at an angle of 13 deg, as suggested in [35]. These two planes were smoothly rounded with a 10 mm radius of bend.

According to the Drude model [36], the gold skin layer in the terahertz range is about 44 nm thick, and the electron free path is 41 nm, which is substantially less than 1 μm. Therefore, the gold layer can be considered a semi-infinite medium. Inside the waveguide, the focused radiation is transformed into waveguide TEM or TM modes and, diffracting in the output waveguide mouth, is converted into SPP. In the experiments, to increase the output intensity, one could change the waveguide gap width δ from half a wavelength to a few wavelengths. According to [28], for metal surfaces coated with micrometer-scale dielectric layers, the conversion efficiency increases substantially, and the strong coupling of SPP to the conductor [10] decreases the radiation losses.

Surface plasmons traveling along a metal–dielectric interface are diffracted at the rectangular edge of the sample, which has a radius of curvature that is much less than the wavelength. To study radiation in the space beyond the end, we applied two detection systems. The first one, shown in Fig. 1(c), was an imaging system consisting of an uncooled microbolometer focal plane array (MBFPA) and a TPX (poly-4-methylpentene-1) lens with a focal length of 50 mm. The MBFPA contains 320×240 microbolometers of 51 μm × 51 μm size (the total size of the array was 16.32 mm × 12.24 mm) and is sensitive to terahertz radiation [37]. The average value of the noise-equivalent power (NEP) of the microbolometer, measured using the NovoFEL radiation, was 2×10^{-10} W/Hz$^{1/2}$ at $\lambda = 140$ μm. The magnification of the optical system in these experiments was $M = b/a = 0.4$. Images were recorded either in the snapshot mode or as a terahertz video with a rate of 15 frames/s.

The second detector [Fig. 1(d)] was a GC-1T Golay cell (NEP $\sim 1.4 \times 10^{-10}$ W/Hz$^{1/2}$) [38] combined with a lock-in amplifier SR-830 (at a 15 Hz chopping frequency). Using this detector, we measured the electromagnetic radiation intensity as a function of the coordinate z for several distances l. The spatial resolution along the z axis was determined by the input slit with a width of 0.2 mm. The polar coordinates for the input slit position are shown in Fig. 1(d).

Most of the experiments were carried out in the configuration shown in Fig. 1(a). Test experiments performed in the reverse-geometry configuration [Fig. 1(b)] confirmed that no BW emitted from the waveguide was observed when the waveguide slit was very small. Increasing the slit led to appearance of the BW, but it was spatially separated from the diffracted wave. Both detector systems in both configurations sensed no radiation in the case of an input wave of TE polarization.

3. DISTRIBUTION OF ELECTROMAGNETIC FIELD INTENSITY BEYOND THE SAMPLE EDGE

Images recorded using the MBFPA with the TPX lens for gold are shown in Fig. 2(a), for gold with a ZnS coating 0.25 μm thick in Fig. 2(b), and with a ZnS coating 0.75 μm thick in Fig. 2(c). The distance a between the sample edge and the lens [Fig. 1(c)] was 175 mm. The scale in Fig. 2 is given for the object plane (at the edge of the sample). Using a blocking half-plane screen, we found that the radiation wavefront at the lens was very narrow, and the diffracted radiation was almost completely captured by the lens aperture with a diameter of 45 mm. The gap width in the waveguide was $\delta \approx 0.25$ mm. Radiation intensity for the bare gold sample was much less than for the ZnS-covered samples, and in this case we had to increase the waveguide gap to $\delta \approx 0.65$ mm. The spatial distribution of radiation emitted from the bare gold surface [see Fig. 2(a)] was wider than that for the ZnS-covered samples. In the latter case we observed a narrow peak near the surface plane but shifted outward by a maximum of 1–2 mm. Intensity variation is also seen in the pictures.

The results obtained with the MBFPA were confirmed in experiments with the Golay cell applied to the sensing of the EMF intensity nearby the sample end [Fig. 1(d)]. Field intensities versus coordinate z measured with the Golay cell at the distance $l = 1$ mm from the edge of the samples are shown in Fig. 3. Behavior of the curves in the figure is similar to those in the graphs in Fig. 2. Some variation can be explained by the difference in the experimental configurations.

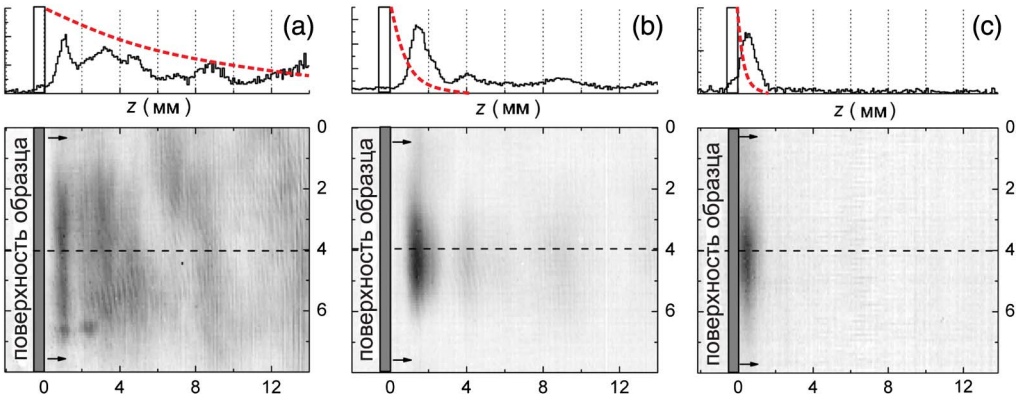

Fig. 2. Images recorded using the MBFPA for (a) gold, (b) gold with a ZnS coating 0.25 μm thick, and (c) gold with a ZnS coating 0.75 μm thick. The scale is given for the object plane. The width of the gap in the waveguide was $\delta \approx 0.65$ μm for image (a) and 0.25 μm for images (b) and (c). Intensities in the graphs are presented in arbitrary units. The dashed red exponential curves are calculated by using the Drude model for the SPP intensity attenuation $\exp(-2z/d_z)$ (see Table 1 in Section 4).

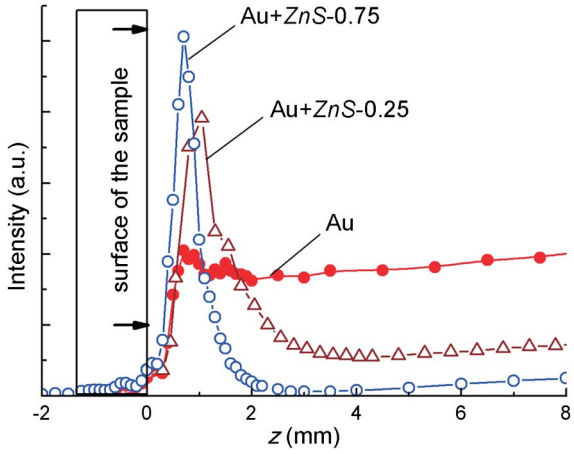

Fig. 3. Field intensities versus coordinate z measured with the Golay cell at the distance $l = 1$ mm from the edge of the sample. Results are given for bare gold and for gold with ZnS coatings 0.75 and 0.25 μm thick. The gap width in the waveguide δ was about 100 μm for gold and 60 μm for gold with ZnS layers.

The MBPFA detected radiation reaching the lens and did not disturb the field near the sample end, whereas the Golay cell with the metal aperture stop with a narrow slit, could disturb the field when situated in the near zone.

From the results presented in this section we may conclude that the radiation emerging when a SPP is diffracted at the rectangular edge of the sample does not exactly conform to an exponentially decaying evanescent SPP field, but the distribution width versus z is qualitatively similar to the behavior of SPP penetration depth in the air, because it is well known [10,39–41] that the penetration depth decreases when the dielectric layer thickness increases.

The following question arises at this point. If we are going to use sensing of diffracted radiation for study of SPP characteristics, how do they correlate with each other? It is evident from the experiments that diffracted waves are somehow connected with SPPs. A quantitative theory of SPP diffraction is presented in the companion paper [34]. A brief overview of portions of this theory that are essential for understanding the experimental data is given in the subsequent sections.

4. THEORY OF SURFACE PLASMON POLARITONS PROPAGATION ALONG METAL–DIELECTRIC–AIR INTERFACES

Let a conductor with the complex dielectric constant ε occupy the lower half-space, $z < 0$, and a transverse magnetic (TM) surface electromagnetic wave propagate in the upper half-space, $z > 0$, along the x axis, as shown in the left-hand half-space in Fig. 4:

$$\begin{aligned}\mathbf{E}(\mathbf{r},t) &= \mathbf{E_0}\,\exp[-\kappa z + i(kx-\omega t)],\\ \mathbf{E_0} &= \{E_{0x},0,E_{0z}\},\\ \mathbf{B}(\mathbf{r},t) &= \mathbf{B_0}\,\exp[-\kappa z + i(kx-\omega t)],\\ \mathbf{B_0} &= \{0,B_{0y},0\}.\end{aligned} \tag{1}$$

The radiation exponentially decays in the z direction with the attenuation coefficient κ, which can be expressed in terms of the given angular frequency ω and the wave vector k. In general, κ is a complex number with a positive real part,

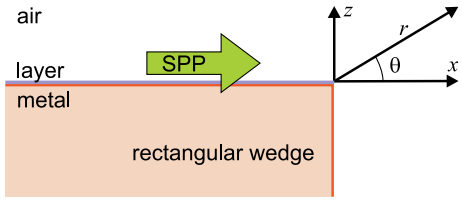

Fig. 4. Schematic of SPP diffraction on a rectangular conducting wedge; the theory predicts the absence of reflected and passed SPPs.

$\mathrm{Re}(\kappa) > 0$. Its reciprocal value determines the field amplitude *decay length* as follows:

$$d_z = [\mathrm{Re}(\kappa)]^{-1}. \tag{2}$$

Similar fields (with a negative attenuation constant, $\mathrm{Re}(\kappa') < 0$) could be written for the lower half-space, but they are needed only for derivation of the dispersion law for the surface wave (see details in [3,5,17,42]),

$$k = k_0\sqrt{\frac{\varepsilon}{1+\varepsilon}}. \tag{3}$$

Here

$$k_0 = \omega/c, \qquad k^2 - \kappa^2 = k_0^2. \tag{4}$$

The Gaussian system of units is used.

Expression (1) can be interpreted as an evanescent wave propagating at a complex angle χ such that

$$k_x = k_0\cos\chi = k, \qquad k_z = -k_0\sin\chi = i\kappa, \qquad \kappa = ik_0\sin\chi. \tag{5}$$

Using the dispersion ratio in Eq. (3) yields

$$\cos\chi = \sqrt{\frac{\varepsilon}{1+\varepsilon}}, \qquad \sin\chi = \sqrt{\frac{1}{1+\varepsilon}}. \tag{6}$$

In a fictitious case of a real ε, there is a surface wave provided that $\varepsilon < -1$. For complex values of ε, there is always a solution with

$$\mathrm{Im}\chi < 0, \tag{7}$$

which decays exponentially with the distance from the conductor boundary. However, speaking about surface waves makes sense only if the propagation length

$$L = [2\,\mathrm{Im}(k)]^{-1} \tag{8}$$

is sufficiently long, i.e., $|\mathrm{Im}(k)| \ll |\mathrm{Re}(k)|$. This condition is certainly satisfied if $|\varepsilon| \gg 1$, which is true for all metals. For gold, for example, at the wavelength $\lambda = 140$ μm, in accordance with many studies summarized in [43], $\varepsilon = -103000 + i\cdot 311000$. Here and below we rounded all numbers to three significant digits. This value, like dielectric functions found for many metals via measurement of their optical properties, is in good agreement with the Drude model. For some metals, introduction of one adjustable parameter in the Drude model appears to be necessary to fit the measurements.

Since for highly conductive metals (Au, Ag, Cu, Al) in the terahertz region the free path of electrons becomes close to

the skin depth, the validity of the Drude approximation must be additionally verified. Analysis of the papers [44–47] in which the surface impedance of gold was examined showed that in the terahertz range the Drude model is in a reasonable agreement with both the kinetic theory of electron collisions [48] and experimental data. This justifies the use of the Drude model as a reasonable approximation in the study below. For bare gold we then obtain

$$\chi = 0.001020 - i \cdot 0.001420,$$
$$k = (44900 + i \cdot 0.065)\mathrm{m}^{-1}, \quad \text{and}$$
$$\kappa = (64 + i \cdot 46)\mathrm{m}^{-1}. \tag{9}$$

Using Eqs. (2), (8), and (9), we find $L = 7.7$ m for the SPP propagation length along the gold–air interface and $d_z = 16$ mm for the decay length at $\lambda = 140$ μm.

As shown in the companion paper [34], for $|\varepsilon| \gg 1$ the dimensionless surface impedance ξ is approximately equal to the parameter χ,

$$\xi = \sin\chi = \sqrt{\frac{1}{1+\varepsilon}} \simeq 0.00102 - i \cdot 0.00142. \tag{10}$$

The surface impedance changes drastically if a dielectric layer is deposited on the metal surface. For a metal–dielectric-film–air composition with a small dielectric film thickness $(1/k_0\sqrt{|\varepsilon|} \ll d \ll \lambda)$ and large dielectric constants for both the metal, $\varepsilon \gg 1$, and the dielectric film, $\varepsilon_\mathrm{d} \gg 1$, we derive

$$\kappa \simeq k_0\left(\frac{1}{\sqrt{-\varepsilon}} + \frac{\varepsilon_d - 1}{\varepsilon_d}k_0 d\right),$$
$$k \simeq k_0\left[1 + \frac{1}{2}\left(\frac{1}{\sqrt{-\varepsilon}} + \frac{\varepsilon_d - 1}{\varepsilon_d}k_0 d\right)^2\right],$$
$$\xi \simeq \frac{1}{\sqrt{\varepsilon}} - i\frac{\varepsilon_d - 1}{\varepsilon_d}k_0 d. \tag{11}$$

Using the dielectric constant for ZnS given in [49], $(\varepsilon_d = 8.7 + i \cdot 0.059)$, we have calculated SPP characteristics for the sample under study, which are presented in Table 1. It would be pertinent to note here that, in accordance with the standard definitions [3,5], we have determined in this paper the propagation length for SPP intensity, but the decay length for SPP field amplitude.

These results clearly demonstrate the feasibility of sensing of thin dielectric films on metals in the terahertz range with the help of surface plasmons. A 0.75 μm ZnS layer on gold, which is only $\sim\lambda/200$ thick decreases by 22 times the SPP decay length in comparison with bare gold. The effect of the dielectric layer on the surface impedance can be estimated [see Eq. (11)] by the following ratio:

$$\left|\frac{\varepsilon_d - 1}{\varepsilon_d}k_0 d\sqrt{\varepsilon}\right| \underset{\varepsilon_d \gg 1}{\longrightarrow} \frac{2\pi d\sqrt{\varepsilon}}{\lambda}. \tag{12}$$

With 0.75 μm ZnS this ratio is equal to 17, and the SPP surface impedance is determined mostly by the dielectric film. With a ZnS layer as thin as 0.25 μm $(\sim\lambda/560)$, in accordance with Eqs. (2) and (11), d_z is three times larger than that with a 0.75 μm layer. The ratio of Eq. (12) lets us estimate the minimum confidently detectable ZnS layer thickness as $d \sim 60$ nm $(\sim\lambda/2300)$.

The calculated propagation lengths given in Table 1 will be compared with the experimental results below (see Section 6). The functions $\exp(-z/d_z)$ with the decay lengths given in Table 1 are inserted into the diagrams in Fig. 2. The characteristic widths of the experimentally recorded intensity distributions of the diffracted waves qualitatively agree with the SPP decay lengths calculated by using the Drude theory, though their profiles differ substantially from the exponential profile. In the next section we will calculate profiles for the diffracted waves and compare them with the experimental ones.

Table 1. Characteristics of SPPs and Diffracted Radiation for Gold and Gold Covered with ZnS Layer Surfaces at $\lambda = 140$ μm (Theory)[a]

Surface	d_z, mm	L, m	$10^3\xi$	R, cm	$\Delta\theta_{fw}$, deg
Au	16	7.7(0.031)	$1.02 - i \cdot 1.42$	1100	0.16
Au–ZnS (0.25 μm)	2	0.95(0.011)	$1.03 - i \cdot 11.3$	17.6	1.3
Au–ZnS (0.75 μm)	0.7	0.34	$1.05 - i \cdot 31.2$	3.3	3.6

[a] d_z, field amplitude decay length; L, propagation length (intensity attenuation length; experimental data, see Section 5, are given in the parentheses); ξ, surface impedance; R, near-field limit; $\Delta\theta_{fw}$, angular divergence in the far field.

5. SURFACE PLASMON POLARITONS DIFFRACTION AT THE SAMPLE END: THEORETICAL PREDICTIONS AND EXPERIMENTAL RESULTS

Now let the metal occupy the quarter plane $x < 0$ and $z < 0$ (the wedge in Fig. 4). When a surface plasmon reaches the end of the sample, it diffracts at the edge. As a result, an EMF must arise beyond the sample end. In the near zone the EMF is dominated by the electric and magnetic components produced directly by electrons oscillating along the metal surface. In this respect, the field induced is somewhat similar to those appearing near a long linear antenna (see [50], Sec. 8.7). In the far-field zone, the EMF is transformed to a free wave. The boundary between near zone and far zone will be defined below.

The problem of SPP diffraction at a rectangular conducting wedge can be exactly solved using the Sommerfeld–Malyuzhinets theory (as mentioned Section 1). A detailed description of the solution technique is given in [34]. It is shown there that the diffracted field is completely described by the magnetic field component transverse to the plane (x, y) of incidence of the surface wave with

$$B_{0y}(r,\theta) = -\frac{1}{2}\exp(-s^2)[-1 + i\,\mathrm{erfi}(s)]\exp(ik_0 r), \tag{13}$$

where $\mathrm{erfi}(s) = (2/\sqrt{\pi})\int_0^s \exp(t^2)\mathrm{d}t$ is the imaginary error function; $s = (\theta + \chi)\sqrt{k_0 r}(1 + i)/2$; $\chi = \arcsin(\xi)$ is the complex angle, which depends on the surface impedance of the top face of the wedge. Equation (13) is valid in both the near and far zones, as well as in the intermediate ("induction" [50]) zone. Note that the result is not sensitive to the surface impedance of the vertical facet, and there are neither reflected nor downward-propagating SPPs, in contrast to the earlier versions of the theory developed in [32,33].

Major conclusions that follow from the theory presented in [34] are listed below.

(1) The incident SPP is completely scattered into a freely propagating electromagnetic wave, and neither the reflected SPP nor the downward-propagating one is excited if the real part of the surface impedance of the top facet of the wedge is positive, $\mathrm{Re}(\xi) > 0$. According to Eqs. (10) and (11), the value of ξ for both bare and ZnS-coated gold meets this condition. This conclusion is very important, but we cannot prove or disprove it within the framework of our experiments.

(2) For a wedge with small surface impedance, the free-wave zone, where the diffracted field of the SPP becomes a freely propagating electromagnetic wave, lies at the distance

$$r \gg R = k_0^{-1}|\mathrm{Im}\,\chi|^{-2}. \tag{14}$$

In the framework of this paper we will use the terms "near" and "far" zones for the distances $x < r$ and $x \gg r$, respectively.

(3) In the far zone, the angular distribution of the diffracted wave has a Lorentzian profile with the divergence

$$\Delta\theta_{fw} = 2|\mathrm{Im}\,\chi| \simeq 2|\mathrm{Im}\,\xi|, \tag{15}$$

which depends on the surface impedance. Here we took into account the small magnitude of the imaginary part of χ; $\mathrm{Im}(\chi) \sim 10^{-3}$–$10^{-2}$ for the samples under study.

(4) The calculated values for R and $\Delta\theta_{fw}$ are given in the last two columns of Table 1. The far zone for the sample with a coating 0.75 μm thick begins at a distance of a few centimeters from the sample edge, whereas for the samples with a coating 0.25 μm thick and for bare gold the far zone shifts to tens of centimeters and tens of meters, respectively. Recall that in the theory we assumed the wedge to be infinite in the y direction, and for a SPP with the width $\Delta y \approx 10$ mm the values for R and $\Delta\theta_{fw}$ have to be recalculated using a 3D approach. However, for the samples with ZnS coatings 0.75 μm thick, the calculated R may be accepted as a good approximation. We will take the values found for bare gold and for the samples with thin layers as reference ones.

(5) The angular patterns of diffracted waves computed by formula (13) for a bare gold substrate and a gold wedge coated with ZnS film are presented in Fig. 5 [34], where the value $|B|^2$ is depicted for several distances from the edge of the sample for parameters relevant to the experiments. It is seen that in the near zone the angular distribution has many peaks, whereas in the far zone (for ZnS covered gold it appears already for $r \geq 10$ mm) the angular distribution gradually converts to a single peak with a Lorentzian-like profile. It will be instructive to compare the far-zone radiation pattern in Fig. 5 with the lobes of a long linear antenna ($L_{\mathrm{ant}} = m\lambda$, $m \gg 1$) (Figs. 8–12 of [50]), which appear to be very similar.

To find the energy flows in the vicinity of the sample end, we have calculated the electric field $\mathbf{E} = (i/k_0)\mathrm{rot}\,\mathbf{B}$ and the Poynting vector $\mathbf{S} \propto \mathbf{E} \times \mathbf{B}^*$. The direction (not value) of the Poynting vector is depicted in Fig. 6 with arrows. The magnitude of the vector is shown by brightness gradations (on a logarithmic scale). The structure of the flows appreciably differs for uncovered and covered gold.

Figures 5 and 6 clearly show that, in accordance with the theory, the total diffracted field is not symmetric about the boundary of the shadow region $\theta = 0$. It extends into the illuminated region $\theta > 0$ much further than into the shadow region $\theta < 0$. The skew is stronger, and the angular variations of intensity are clearly seen, for bare gold. This assertion agrees with the experimentally observed variations of intensity shown in Figs. 2 and 3. Another important conclusion is that the radiation intensity in the illuminated area does not copy the profile of the surface wave: instead of monotonically decreasing with the distance from the face of the wedge, at first it grows and only then decays. Again, this fact was confirmed experimentally (Figs. 2 and 3), which shows that

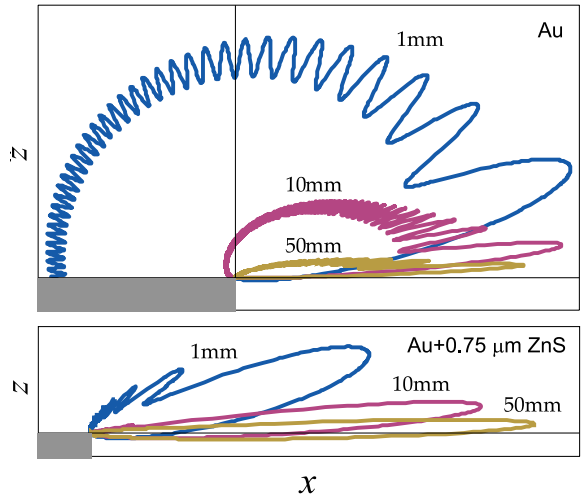

Fig. 5. Angular pattern of the value $|B|^2$ for SPP diffracted by a bare gold wedge and a gold wedge coated with 0.75 μm ZnS film; $\lambda = 140$ μm; the curves correspond to three distances r from the origin (see the coordinate system in Fig. 1).

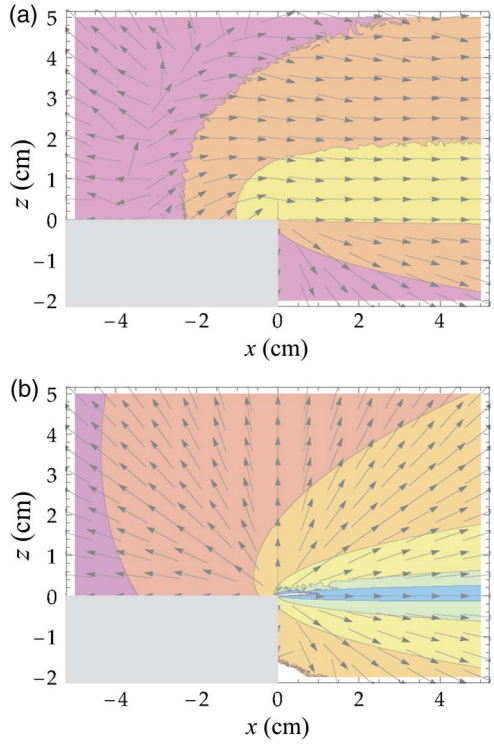

Fig. 6. EMF characteristics in the vicinity of conductive wedges: (a) bare gold and (b) gold +0.75 μm ZnS. The arrows indicate the direction of the Poynting vector; the color map shows the magnitude of the Poynting vector (gradations are given on a logarithmic scale); $\lambda = 140$ μm.

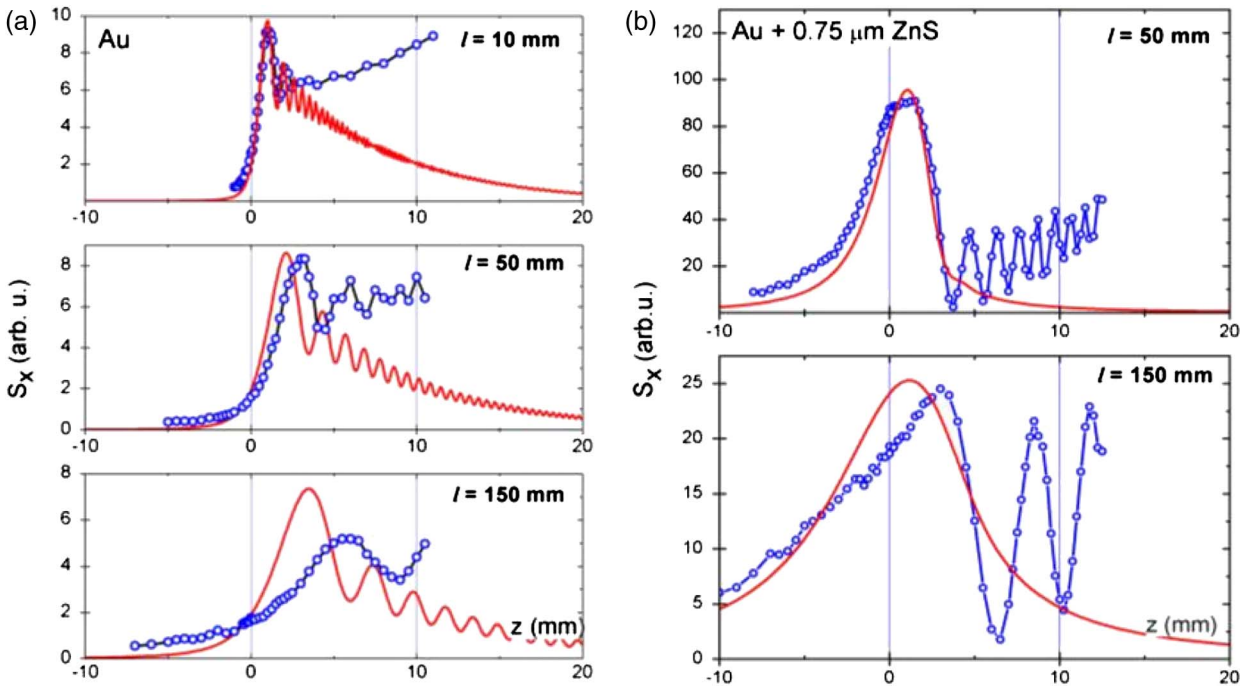

Fig. 7. Field intensity versus angle θ at different distances from the sample edge: (a) bare gold and (b) gold +0.75 μm ZnS coating. The dots show the experimental data measured using the Golay cell; the curves are the theoretical calculations of the x component of the Poynting vector.

an incident surface wave is mainly scattered into the upper hemisphere.

For more detailed comparison of the theory with experimental results, we carried out additional Golay-cell measurements of diffracted field angular distribution at different distances l [see Fig. 1d)] from the sample. Results are presented in Fig. 7. In close vicinity to the wedge ($l = 10$–50 mm) and for small z values, the measured intensity for both bare gold and ZnS-covered samples is in rather good agreement with the theoretical predictions. For a distance of 150 mm, where the 2D approximation cannot be applied, the difference between the experiment and theory becomes apparent. The 2D approximation breaks down at distances substantially longer than the laser beam (and SPP) width $\Delta y \approx 10$ mm and comparable with the sample length, which is equal to 170 mm. At higher z values, an obvious disagreement between patterns obtained with the Golay cell and the MBFPA is seen. We associate the Golay-cell recorded growth of intensity with increasing coordinate z with the electric field perturbation and multiple reflections arising when the metal screen with a narrow slit mounted at input horn of the Golay cell enters into the EMF.

(6) The diffracted field does not depend on the surface impedance of the right (vertical) facet of the wedge. Experiments with samples with bare and gold-covered right facets of glass substrate (Fig. 8) confirmed this assertion. Indirectly, it supports the assertion of absence of downward-propagating SPPs.

6. SURFACE PLASMON POLARITON PROPAGATION LENGTH

The theory described in the two previous sections and the experimental results, which confirmed the main results of the theory, justify the feasibility of measuring SPP intensity from the intensity of wave diffracted at a rectangular wedge. Since the theory predicts complete transformation of SPPs into diffracted waves, one can assume that field intensity at a reasonable distance from the sample edge (see the previous section) is proportional to SPP intensity. The high directionality of the diffracted wave enables practically complete capture of the wave power.

We studied the decay of intensity of SPPs propagating along a metal–dielectric interface with a 45 deg gold mirror M_3 deposited on a glass prism, as shown in Fig. 1(d). Using an imaging system with a focal plane array microbolometer, we showed the mirror to be an absolute equivalent of the rectangular wedge as concerns the diffraction task. Images recorded for the same samples were identical to the intensity distributions shown in Fig. 2. For the sake of simplicity, in subsequent experiments we set the Golay cell at the distance of $l' = 50$ mm from the sample surface and used it as a detector [Fig. 1(d)]. Once more, the intensity distributions were the same as in Fig. 3. The total diffracted wave energy was calculated by integration of the intensity distribution over the coordinate z' at each mirror position x on the sample.

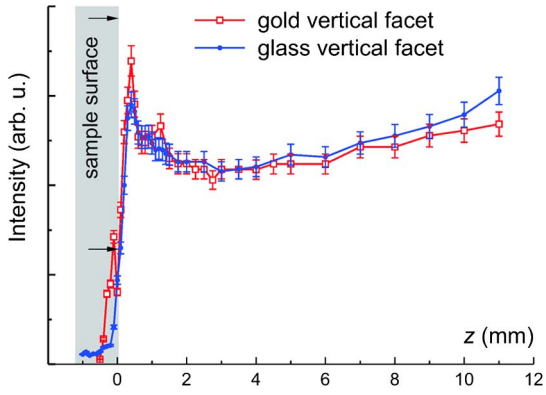

Fig. 8. Diffracted field intensity as a function of z measured with the Golay cell at the distance $l = 1$ mm for the bare gold samples with gold-coated and uncoated right facet.

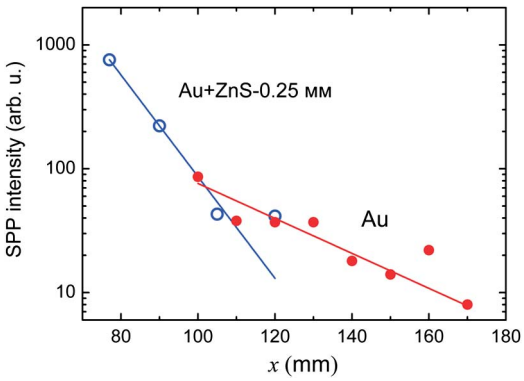

Fig. 9. SPP intensity versus path length measured with the Golay cell for the bare gold and for the gold coated with a 0.25 μm ZnS layer; the distance l' (see Fig. 1) was 50 mm; $\lambda = 140$ μm. Points, experiment; curves, exponential fit.

Assuming that surface characteristics are uniform along the sample, we took the energies measured at each point x proportional to the SPP intensity. Figure 9 shows the results of the measurements for bare gold and gold with a 0.25 μm layer of ZnS. Intensity fluctuations for bare gold may be associated with the interference of the SPP and a weak BW leaking from the output mouth of the waveguide (see Fig. 1). The propagation length for bare gold was $L = 31 \pm 6$ mm, while for gold with the ZnS layer it was only $L = 11 \pm 1$ mm.

The experimentally measured SPP propagation lengths are a few orders of value less than the calculated ones (see Table 1). Such a large discrepancy between the theory and experiment was observed by many authors [9,20,35,40,41,51–54]. In [41], for example, it was found that covering an aluminum surface with a germanium layer of submicrometer thickness decreased this difference, and for a thickness of more than 2 μm the calculated and experimental values of L were nearly equal (see Table 3 of [41]). In the present experiments, the difference between the experimental and the theoretical values of L for gold with 0.25 μm thick ZnS coating also decreased three times as compared with bare gold. Causes of this disagreement between the theory and experiments have been widely discussed (radiation loss, surface nonuniformities, absorption in adsorbed water, etc.), but no satisfying explanation has been presented yet.

7. CONCLUDING REMARKS

In this paper we have studied, both experimentally and theoretically, propagation of SPPs along a plane metal–dielectric–air interface and their diffraction at the surface edge. In contrast to most studies carried out using the time-domain technique, we launched the plasmons using the monochromatic radiation of the high-power NovoFEL. This enabled us, first, to apply real-time detectors to radiation sensing; second, to obtain results directly without the necessity of solving the inverse problem; and third, to get rid of the problems related to SPP dispersion. In other words, our results are in many aspects complementary to the previously obtained ones.

An imaging system consisting of a lens with a MBFPA and one-channel Golay cell detector enabled us to examine the EMF arising at SPP diffraction at the edge. The experimentally recorded intensity distribution of the diffracted wave in the direction normal to the surface differed from the evanescence wave distribution in the SPPs, but their characteristic widths were practically the same and correlated with the calculations made within the framework of the Drude model.

The good agreement of the theory with the experiment is promising for simulations of SPP-based terahertz optoelectronic devices. The narrow angular distribution of diffracted radiation that was found in this paper partially explains the "jumping" of SPPs through gaps, which was observed in a number of recent papers [22,54–56]. This fact may also be applied to development of SPP optoelectronic devices with air gaps. The strong effect produced by a thin dielectric layer on the decay length allows development of techniques for thin film and dispersed substance detection and spectroscopy.

In this paper we have confirmed the well-known fact, which, however, still has no clear explanation, of extremely short SPP propagation length in the terahertz region, which disagrees with the Drude model, while the decay length is in good agreement with the theory. Here we resist the temptation to try to explain this fact, but we will return to this problem in our future experiments. It is important that the NovoFEL radiation can be precisely tuned to any wavelength within 50–240 μm. Since the propagation length at $\lambda = 140$ μm is much smaller than the calculated one, whereas in the visible range it is are practically identical, decreasing wavelength, say to 50 μm, may paradoxically increase the SPP propagation length, which is favorable for optical communication technologies.

ACKNOWLEDGMENTS

This work was partially funded by the Russian Government, grant 11.G34.31.0033, the Russian Foundation for Basic Research, grants 11-02-12252-ofi-m, 11-02-12171-ofi-m, and the Russian Ministry of Education and Science, state contracts 14.B37.21.0732, 14.B37.21.0784, and 14.B37.21.0750. The experiments were carried out using equipment belonging to the SCSTR.

REFERENCES

1. G. N. Zhizhin, O. I. Kapusta, M. A. Moskaleva, V. G. Nazin, and V. A. Yakovlev, "Surface wave spectroscopy and properties of the surface," Sov. Phys. Usp. **18**, 927–928 (1975).
2. G. N. Zhizhin, M. A. Moskaleva, E. V. Shomina, and V. A. Yakovlev, "Surface electromagnetic wave propagation on metal surfaces," in *Surface Polaritons. Electromagnetic Waves at Surfaces and Interfaces*, V. M. Agranovich and D. L. Mills, eds. (North-Holland, 1982), chap. 3.
3. H. Raether, *Surface Plasmons on Smooth and Rough Surfaces and on Gratings* (Springer-Verlag, 1988).
4. L. Novotny and B. Hecht, *Principles of Nano-Optics* (Cambridge University, 2006).
5. S. A. Maier, *Plasmonics: Fundamentals and Applications* (Springer, 2007).
6. A. Sommerfeld, "Fortpflanzung electrodynamischer Wellen an einem zylindrischen Leiter (Transmission of electrodynamic waves along a cylindrical conductor)," Ann. Phys. (Berlin) **303**, 233–290 (1899).
7. J. Zenneck, "Über die Fortpflanzung ebener elektromagnetischer Wellen läangs einer ebenen Leiterfläache und ihre Beziehung zur dratlosen Telegraphie (On the propagation of plane electromagnetic waves along a planar conductor surface and its relationship to wireless telegraphy)," Ann. Phys. Ser. 4 **23**, 848–866 (1907).
8. R. T. Ling, J. D. Scholler, and P. Ya. Ufimtsev, "The propagation and excitation of surface waves in an absorbing layer," Prog. Electromagn. Res. **19**, 49–91 (1998).

9. T.-I. Jeon and D. Grischkowsky, "THz Zenneck surface wave THz surface plasmon propagation on a metal sheet," Appl. Phys. Lett. **88**, 061113 (2006).
10. M. Gong, T.-I. Jeon, and D. Grischkowsky, "THz surface wave collapse on coated metal surfaces," Opt. Express **17**, 17088–17101 (2009).
11. A. V. Kukushkin, A. A. Rukhadze, and K. Z. Rukhadze, "On the existence conditions for a fast surface wave," Phys. Usp. **55**, 1124–1133 (2012).
12. U. Fano, "The theory of anomalous diffraction gratings and of quasi-stationary waves on metallic surfaces (Sommerfeld's waves)," J. Opt. Soc. Am. **31**, 213–222 (1941).
13. F. Yang, J. R. Sambles, and G. W. Bradberry, "Long-range surface modes supported by thin films," Phys. Rev. B **44**, 5855–5872 (1991).
14. J. F. O'Hara, W. Withayachumnankul, and I. Al-Naib, "A review on thin-film sensing with terahertz waves," Int. J. Infrared Millim. Waves **33**, 245–291 (2012).
15. S. S. Attwood, "Surface-wave propagation over a coated plane conductor," J. Appl. Phys. **22**, 504–509 (1951).
16. P. Dawson, F. de Fornel, and J.-P. Goudonett, "Imaging of surface plasmon propagation and edge interaction using a photon scanning tunneling microscope," Phys. Rev. Lett. **72**, 2927–2930 (1994).
17. B. A. Knyazev and A. V. Kuzmin, "Surface electromagnetic waves: from visible range to microwaves," Vestn. Novosib. State Univ. Phys. **2**, 108–122 (2007) (in Russian).
18. J. Lloyd-Hughes and T.-I. Jeon, "A review of the terahertz conductivity of bulk and nano-materials," Int. J. Infrared Millim. Waves **33** 871–925 (2012).
19. R. J. Seymour, E. S. Koteles, and G. I. Stegeman, "Far-infrared surface plasmon coupling with overcoated gratings," Appl. Phys. Lett. **41**, 1013–1015 (1982).
20. K. W. Steijn, R. J. Seymour, and G. I. Stegeman, "Attenuation of far-infrared surface plasmons on overcoated metal," Appl. Phys. Lett. **49**, 1151–1153 (1986).
21. J. Saxler, J. G. Rivas, C. Janke, H. P. M. Pellemans, P. H. Bolivar, and H. Kurz, "Time-domane measurements of surface plasmon polaritons in the terahertz frequency range," Phys. Rev. B **69**, 155427 (2004).
22. M. Nazarov and J.-L. Coutaz, "Terahertz surface waves propagating on metals with sub-wavelength structure and grating reliefs," Int. J. Infrared Millim. Waves **32** 1054–1073 (2011).
23. N. A. Vinokurov, E. N. Dementyev, B. A. Dovzhenko, A. A. Galt, Ya. V. Getmanov, B. A. Knyazev, E. I. Kolobanov, V. V. Kubarev, G. N. Kulipanov, L. E. Medvedev, S. V. Miginsky, L. A. Mironenko, V. K. Ovchar, B. Z. Persov, V. M. Popik, T. V. Salikova, M. A. Scheglov, S. S. Serednyakov, O. A. Shevchenko, A. N. Skrinsky, V. G. Tcheskidov, M. G. Vlasenko, P. Vobly, and N. S. Zaigraeva, "Status and prospects of the Novosibirsk FEL facility," in *Proceedings of XXII Russian Particle Accelerator Conference*, *RuPAC-2010*, Protvino, Russia, 2010, Sept. 27–Oct. 1 (RAS, 2010), pp. 133–135.
24. B. A. Knyazev, G. N. Kulipanov, and N. A. Vinokurov, "Novosibirsk terahertz free electron laser: instrumentation development and experimental achievements," Meas. Sci. Technol. **21**, 054017 (2010).
25. K. J. Ahn, K. G. Lee, H. W. Kihm, M. A. Seo, A. J. L. Adam, P. C. M. Planken, and D. S. Kim, "Optical and terahertz near-field studies of surface plasmons in subwavelength metallic slits," New J. Phys. **10**, 105003 (2008).
26. R. Mueckstein and O. Mitrofanov, "Imaging of terahertz surface plasmon waves excited on a gold surface by a focused beam," Opt. Express **19**, 3212–3217 (2011).
27. T. Okada, M. Nagai, and K. Tanaka, "Resonant phase jump with enhanced electric field caused by surface phonon polariton in terahertz region," Opt. Express **16**, 5633–5641 (2008).
28. R. J. Seymour, J. J. Krupczak, and G. I. Stegeman, "High efficiency coupling to the overcoated surface plasmon mode in the far infrared," Appl. Phys. Lett. **44**, 373–375 (1984).
29. G. Chartier, K. J. Woo, E. Pic, R. Reinisch, and G. Voirin, "Diffraction d'une onde électromagnétique de surface par l'extrémité du support de propagation," J. Phys. **45**, 429–433 (1984).
30. R. F. Wallis, A. A. Maradudin, and G. I. Stegeman, "Surface plasmon reflection and radiation at end faces," Appl. Phys. Lett. **42**, 764–766 (1983).
31. A. A. Maradudin, R. F. Wallis, and G. I. Stegeman, "The optics of surfaces and guided wave polaritons," Prog. Surf. Sci. **33** 171–257 (1990).
32. H. A. Jamid and S. J. Al-Bader, "Diffraction of surface plasmon-polaritons in an abruptly terminated dielectric–metal interface," IEEE Photon. Technol. Lett. **7** 321–323 (1995).
33. V. B. Zon, "Reflection, refraction, and transformation into photons of surface plasmons on a metal wedge," J. Opt. Soc. Am. B **24**, 1960–1967 (2007).
34. I. A. Kotelnikov, V. V. Gerasimov, and B. A. Knyazev, "Diffraction of surface wave on conducting rectangular wedge," Phys. Rev. A **87**, 023828 (2013).
35. E. S. Koteles and W. H. McNeill, "Far infrared surface plasmon propagation," Int. J. Infrared Millim. Waves **2**, 361–371 (1981).
36. N. W. Ashkroft and N. D. Mermin, *Solid State Physics* (Harcourt, 1976).
37. M. A. Dem'yanenko, D. G. Esaev, I. V. Marchishin, V. N. Ovsyuk, B. I. Fomin, B. A. Knyazev, and V. V. Gerasimov, "Application of uncooled microbolometer detector arrays for recording radiation of the terahertz spectral range," Optoelectron. Instrum. Data Process. **47**, 109–113 (2011).
38. Tydex., "Golay cells," http://www.tydexoptics.com/en/products/thz_optics/golay_cell/.
39. I. Pockrand, "Surface plasma oscillations at silver surfaces with transparent and absorbing coatings," Surf. Sci. **72**, 577–588 (1978).
40. Z. Schlesinger and A. J. Sievers, "IR surface-plasmon attenuation coefficients for Ge-coated Ag and Au metals," Phys. Rev. B **26**, 6444–6454 (1982).
41. G. N. Zhizhin, A. K. Nikitin, G. D. Bogomolov, V. V. Zavialov, Y. U. Jeong, L. B. Cheol, S. H. Park, and H. J. Cha, "Absorption of surface plasmons in a metal-cladding layer-air structure in the terahertz frequency range," Opt. Spectrosc. **100**, 734–738 (2006).
42. V. V. Klimov, *Nanoplasmonics* (Fizmatlit, Moscow, 2009) (in Russian).
43. M. A. Ordal, L. L. Long, R. J. Bell, S. E. Bell, R. R. Bell, R. W. Alexander, Jr., and C. A. Ward, "Optical properties of the metals Al, Co, Cu, Fe, Pb, Ni, Pd, Pt, Ag, Ti, and W in the infrared and far infrared," Appl. Opt. **22**, 1099–1119 (1983).
44. G. E. H. Reuter and E. H. Sondheimer, "The theory of the anomalous skin effect in metals," Proc. R. Soc. A **195**, 336–364 (1948).
45. R. B. Dingle, "The anomalous skin effect and reflectivity of metals," Physica **19**, 311–347 (1953).
46. C. G. Malone, "A technique for the measurement of the far-infrared radiative properties of metal and superconductor thin films," Ph.D. thesis (Massachusetts Institute of Technology, 1997).
47. G. Brandli and A. J. Sievers, "Absolute measurement of the far-infrared surface resistance of Pb," Phys. Rev. B **5**, 3550–3557 (1972).
48. J. M. Ziman, *Electrons and Phonons* (Oxford University, 1960).
49. E. D. Palik, ed., *Handbook of Optical Constants of Solids* (Academic, 1998).
50. J. B. Marion, *Classical Electromagnetic Radiation* (Academic, 1965).
51. D. L. Begley, R. W. Alexander, C. A. Ward, R. Miller, and R. J. Bell, "Propagation distances of surface electromagnetic waves in the far infrared," Surf. Sci. **81**, 245–251 (1979).
52. L. S. Mukina, M. M. Nazarov, and A. P. Shkurinov, "Propagation of THz plasmon pulse on corrugated and flat metal surface," Surf. Sci. **600**, 4771–4776 (2006).
53. M. Martl, J. Darmo, K. Unterrainer, and E. Gorni, "Excitation of terahertz surface plasmon polaritons on etched groove gratings," J. Opt. Soc. Am. B **26**, 554–558 (2009).
54. M. Nazarov, F. Garet, D. Armand, A. Shkurinov, and J.-L. Coutaz, "Surface plasmon THz waves on gratings," C.R. Physique **9**, 232–247 (2008).
55. M. Nazarov, J.-L. Coutaz, A. Shkurinov, and F. Garet, "THz surface plasmon jump between two metal edges," Opt. Commun. **277**, 33–39 (2007).
56. R. A. Flynn, I. Vurgaftman, K. Bussmann, B. S. Simpkins, Ch. S. Kim, and J. P. Long, "Transmission efficiency of surface plasmon polaritons across gaps in gold waveguides," Appl. Phys. Lett. **96**, 111101 (2010).